Proc. Natl. Acad. Sci. USA
Vol. 86, pp. 2190–2194, April 1989
Biophysics

Crystal structure of core streptavidin determined from multiwavelength anomalous diffraction of synchrotron radiation

(biotin/avidin/selenium/x-ray crystallography)

WAYNE A. HENDRICKSON[†], ARNO PÄHLER[†], JANET L. SMITH[†‡], YOSHINORI SATOW[§¶], ETHAN A. MERRITT[‖††], AND R. PAUL PHIZACKERLEY[‖]

[†]Howard Hughes Medical Institute, Department of Biochemistry and Molecular Biophysics, Columbia University, New York, NY 10032; [§]Photon Factory, National Laboratory for High Energy Physics, Oho, Tsukuba-shi, Ibaraki 305, Japan; and [‖]Stanford Synchrotron Radiation Laboratory, Stanford University, Stanford, CA 94305

Communicated by Jerome Karle, November 9, 1988 (received for review September 28, 1988)

ABSTRACT **A three-dimensional crystal structure of the biotin-binding core of streptavidin has been determined at 3.1-Å resolution. The structure was analyzed from diffraction data measured at three wavelengths from a single crystal of the selenobiotinyl complex with streptavidin. Streptavidin is a tetramer with subunits arrayed in D_2 symmetry. Each protomer is an 8-stranded β-barrel with simple up-down topology. Biotin molecules are bound at one end of each barrel. This study demonstrates the effectiveness of multiwavelength anomalous diffraction (MAD) procedures for macromolecular crystallography and provides a basis for detailed study of biotin–avidin interactions.**

Streptavidin takes its name from the bacterial source of the protein, *Streptomyces avidinii*, and from hen egg-white avidin with which it shares an extraordinary ligand binding affinity ($K_d \approx 10^{-15}$ M) for biotin (1). This similarity extends to many other properties (2), including a common tetrameric structure and a 33% identity in amino acid sequence between avidin and the homologous core of streptavidin (3, 4). Core streptavidin is proteolyzed naturally, but not always completely (3), at both ends of the 159-residue gene product to a 125- to 127-residue core (4) that matches quite precisely with the actual secreted avidin gene product (5). The biological functions of avidin and streptavidin are poorly understood, but they most probably involve antibiotic properties. Interest in the avidin family, however, transcends their natural biology. Their remarkable avidity for biotin motivates two types of study: (*i*) efforts to understand the chemical basis for the high affinity and (*ii*) attempts to optimize biotechnology applications that exploit this activity (6–8). We aim to examine these biophysical and biotechnological properties in refined crystallographic detail. Streptavidin has also been crystallized by others (ref. 9 and P. McLaughlin, personal communication).

This structural study of streptavidin also has a second objective related to diffraction methodology. It seemed from the outset that selenobiotinyl streptavidin could be an apt subject for direct analysis from multiwavelength anomalous diffraction (MAD) data obtained with synchrotron radiation. Selenobiotin is a stable compound (10) sufficiently similar to biotin itself that the two molecules crystallize isomorphously (11). The high affinity ($K_d \approx 10^{-13}$ M) of avidin for desthiobiotin (2, 12) suggested to us that selenobiotin would also bind well. We expected anomalous diffraction ratios (13) from the four selenium atoms in the 54-kDa core streptavidin tetramer (up to 3%) that compared favorably with signals measured successfully from crambin (14) and myohemerythrin (15) and with those obtained in our lamprey hemoglobin test of MAD phasing (16, 17).

The theoretical basis for the MAD method and details of its implementation are presented elsewhere (13, 17, 18). Qualitatively, MAD experiments can be thought of as *in situ* multiple isomorphous replacements (MIR) generated by the variation in scattering factors that accompanies change of wavelength. Unlike MIR, however, here isomorphism is perfect and a single crystal can suffice. The potential for such experiments has long been recognized (19), but effective use awaited synchrotron radiation and algebraic methods (13, 18) that facilitate the analysis of MAD data. Results from such experiments are beginning to appear (17, 20–24). Most of these studies also incorporate phase information from other sources, and all pertain to proteins that belong to families of known structure. Since streptavidin is unrelated to any molecules of known three-dimensional structure, this application based exclusively on MAD phasing represents a stringent test of the method. Preliminary accounts of this work have been presented (4, 25, 26).

MATERIALS AND METHODS

Crystals of Selenobiotinyl Streptavidin. Core streptavidin crystals of type C1 (4) were grown from material supplied by Celltech (Berkshire, U.K.). These crystals were stabilized in a medium of 40% saturated ammonium sulfate in 0.1 M potassium acetate that was saturated with respect to selenobiotin and adjusted to pH 5.0 [for the Stanford Synchrotron Radiation Laboratory (SSRL)] or pH 4.3 (for the Photon Factory). Selenobiotin for the SSRL experiment was a gift from A. Marquet (Université Pierre et Marie Curie, Paris), and that for the Photon Factory experiment was the gift of J. Blount from a Hoffman–La Roche synthesis. C1 crystals are in space group *I222*. The lattice dimensions are $a = 95.20$ Å, $b = 105.63$ Å, and $c = 47.41$ Å for the SSRL data crystal as measured with CuKα radiation after return from Stanford and $a = 95.27$ Å, $b = 105.41$ Å, and $c = 47.56$ Å for the Photon Factory crystal as measured at the synchrotron.

SSRL Experiments. The experiments at SSRL were conducted as in our study of lamprey hemoglobin (17) using the area detector facility (27) on beamline I-5. The storage ring was operated at 3.0 GeV with electron currents up to 80 mA. X-rays of ≈2-eV bandpass from double Ge(111) crystals, detuned by ≈10% for rejection of harmonics, were used

The publication costs of this article were defrayed in part by page charge payment. This article must therefore be hereby marked "*advertisement*" in accordance with 18 U.S.C. §1734 solely to indicate this fact.

Abbreviations: MAD, multiwavelength anomalous diffraction; MIR, multiple isomorphous replacement; SSRL, Stanford Synchrotron Radiation Laboratory.

[‡]Present address: Department of Biological Sciences, Purdue University, West Lafayette, IN 49907.
[¶]Present address: Faculty of Pharmaceutical Sciences, University of Tokyo, Hongo, Bunkyo-ku, Tokyo 113, Japan.
[††]Present address: Department of Biological Structure, University of Washington, Seattle, WA 98105.

without focusing. The x-ray energy was calibrated as 11921.1 eV at the inflection point of L_{III} absorption through a 10-μm gold foil. X-ray absorption spectra were measured by fluorescence detected with a scintillation counter placed near the crystal and normalized by an incident intensity monitor. The area detector was placed at 598 mm for diffraction measurements from a large crystal (1.14 × 0.42 × 0.17 mm at extremes) oriented with the [011] direction along the goniometer φ axis. The diffraction protocol was designed to record Bijvoet mates with equivalent absorption paths and to acquire all data pertinent to a given phase (Bijvoet mates at every wavelength) close together in time. Rotations of 102° were made about φ at $\chi = 0$ in "inverse beam" settings (φ and $\varphi + \pi$) to obtain Bijvoet mates and in a limited range of 64.4° in ω rotations at $\chi = -90°$ about a^* to give mirror-related Bijvoet mates. Due to broad reflection profiles, integration frames of 0.25° and 0.20° were used in the respective settings at $\chi = 0°$ and $-90°$. Frames of data were collected alternately among four wavelengths: 1.1000 Å, 0.9792 Å, 0.9789 Å, and 0.9000 Å. The crystal was maintained at 4°C throughout the 5 days of data collection.

Photon Factory Experiments. Experiments at the Photon Factory were conducted on the diffractometer facility on beamline 14A (28) using radiation from a superconducting vertical wiggler in the storage ring, which was operated at 2.5 GeV with currents from 250 to 120 mA. Monochromatic x-rays were produced with a fixed exit Si(111) double-crystal system and then focused by a platinum-coated fused quartz mirror. X-ray energies were reckoned from an absolute calibration of monochromator angles and the Si(111) *d*-spacing. A single crystal with extreme dimensions of 0.58 × 0.30 × 0.10 mm was illuminated from 0.8-mm aperture. X-ray absorption spectra, measured by fluorescence with a scintillation detector, were used to select monochromator setting angles for the diffraction measurements. These angles correspond to wavelengths of 0.9809 Å at the average inflection point, 0.9795 Å at the average peak value, and 0.9000 Å at a remote point. Diffraction data were measured with a single counter from full width (0.6°) ω scans at 8°/min with 1-sec background counts at each end of the reflection profile. Rather wide scans were required because of peak splitting. The data were collected in shells starting from low scattering angles with a succession of the three wavelengths within each shell. Friedel mates were scanned alternately in blocks of 20 reflections. The temperature at the crystal remained constant at 26°C as the crystal was exposed for 97 hr over the course of 8 days that included a 1-day wiggler failure and a 2.5-day planned shutdown.

Scattering Factor Evaluation. The x-ray fluorescence data measured at SSRL were processed into scattering factors as described (17). Atomic absorption spectra are fitted to theoretical values outside the immediate edge region. Imaginary components of anomalous scattering, f'', follow by direct proportion and real components, f', derive from Kramer–Kronig transformation. Scattering factors for the Photon Factory experiments were obtained by least-squares evaluation in a MAD fitting program (Y.S., unpublished results).

Diffraction Data Processing. Diffraction data from SSRL were reduced to integrated intensities by using SSRL software developed by one of us (E.A.M.), but with some modifications due to broad reflection profiles caused by crystal cracks. Local scaling procedures used previously were supplemented by special treatments, dependent on rotation angle φ and on diffracted intensity, to cope with exceptional systematic errors, especially for the inverse beam data. Photon Factory data were reduced with a program by one of us (Y.S.) that corrects for various factors including background, attenuator absorption, beam monitor normalization, standards normalization, ψ-scan absorption correction, and Lorentz and polarization factors. These reduced data were placed on a quasi-absolute scale and also corrected for radiation damage by scaling in shells to a unique set of rapidly measured CuKα data scaled by Wilson's statistics. Parameterized local scaling (14) adjustments were relatively slight—not larger than 2.2% for Bijvoet pairs and 3.0% between wavelengths (1.4% and 1.1%, respectively, for the 3.3-Å data).

MAD Phasing Analysis. Phase evaluation was based on the algebraic analysis of MAD data introduced by Karle (18) and implemented, in somewhat different form, in a least-squares program MADLSQ (13, 17). Wavelength-dependent factors due to anomalous scattering are separated from the variables due exclusively to the wavelength-independent normal scattering. Thus, given anomalous scattering factors $f'(\lambda)$ and $f''(\lambda)$, the MAD structure factor amplitudes $|^{\lambda}\mathbf{F}(\mathbf{h})|$ measured with standard deviation σ_F for Bijvoet pairs of reflections, $\pm\mathbf{h}$, at each wavelength λ, are fitted by three parameters common to the set of intensities for this **h**. These are the structure factor amplitudes due to the normal scattering contributions from anomalous centers, $|^{\circ}F_A|$, and from the entire structure, $|^{\circ}F_T|$, as well as the phase difference for these contributions, $\Delta\varphi = {}^{\circ}\varphi_T - {}^{\circ}\varphi_A$. The structure of anomalous centers is deduced from the $|^{\circ}F_A|$ values, in this case using Patterson syntheses and $^{\circ}\varphi_A$ values are then calculated from this structure. The phases needed for a Fourier synthesis can then be readily evaluated from $^{\circ}\varphi_T = \Delta\varphi + {}^{\circ}\varphi_A$. Here, a phase probability analysis was devised to prepare *ABCD* coefficients for phase combination (29) in molecular averaging. Molecular averaging refinement was done with our AVGSYS program system.

Model Fitting and Refinement. Electron-density distributions for the crystal were transformed into the molecular frame of reference (4), and contoured sections of the Photon Factory map were displayed on transparent sheets at a scale of 4 Å/cm. An interpretation into α-carbon chain tracings was made by visual inspection. FRODO (30) was used to fit a full atomic model into density. The model was optimized by stereochemically restrained refinement (31) against $|^{\circ}F_T|$ values.

RESULTS AND DISCUSSION

Anisotropy of Anomalous Scattering. High-resolution x-ray absorption spectra measured at SSRL were scanned from 11.3 to 13.8 keV from crystals oriented with the electric vector **E** of the x-ray beam set parallel with each of the three crystal axes. Scattering factors fitted to these spectra show pronounced anisotropy near the absorption edge (Fig. 1). The edge positions as defined by minimal f' are at 6, 1, and 2 eV above the elemental absorption edge for **E** parallel to **a**, **b**, and **c**, respectively, and the strength of the "white lines" at maximal f'' also varies markedly. Absorption spectra measured with **E**$\parallel$**a** and **E**$\parallel$**c** from the Photon Factory crystal also had a 4- to 5-eV displacement in edge position, but white-line features were greatly reduced due to the limited energy resolution (≈10 eV).

Anomalous scattering factors for use in phase determinations were taken as the average of the unique anisotropic values near the edge and as theoretical values at remote points. Scattering factors (f', f'') obtained for the SSRL data are (−1.622, 3.285) at 0.9000 Å, (−7.623, 5.083) at 0.9789 Å, (−9.203, 4.382) at 0.9792 Å, and (−1.958, 0.617) at 1.1000 Å. Near-edge scattering factors obtained by a least-squares evaluation of the Photon Factory diffraction data are (−6.203, 3.663) at 0.9795 Å and (−8.198, 2.058) at 0.9809 Å. Discrepancies in edge wavelengths as defined at the two synchrotrons must be ascribed to calibration differences. The pleiochroism of these crystals is similar to that found for monoclinic selenolanthionine (32); this suggested biotin ori-

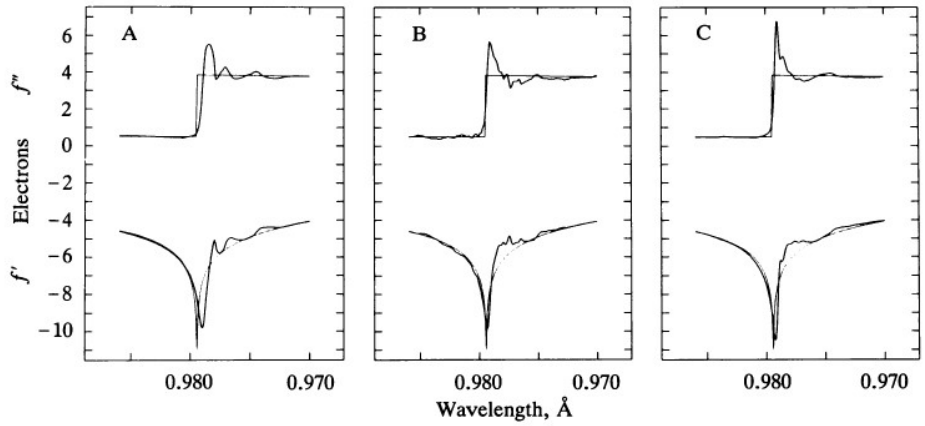

FIG. 1. Anisotropy in anomalous scattering factors for selenium in selenobiotinyl streptavidin. (*A–C*) Spectra (thick lines) measured with the electric vector **E** parallel with crystal axes **a**, **b**, and **c**, respectively. Theoretical values for elemental selenium are shown as thin lines. Values of f'' (upper traces) and f' (lower traces) in electrons are plotted as a function of decreasing wavelengths in Å.

entations with axis **a** nearly perpendicular to the C-Se-C plane and with axis **c** contained in it. Indeed, the average plane normal in our latest model makes angles of 28°, 66°, and 78° with axes **a**, **b**, and **c**, respectively.

Selenium Positions. The selenium positions were deduced from Patterson syntheses based on the SSRL data. These diffraction measurements out to Bragg spacings of 3.0 Å were reduced and scaled to produce 10,481 reflection sets of Bijvoet pairs at four wavelengths (not always complete). The $|^{\lambda}F(\pm\mathbf{h})|$ data for each unique reflection were fitted with MADLSQ and the results were merged into a unique set of 5047 of the possible 5050 reflections corresponding to 3-Å resolution. The merging R-value based on $|^{\circ}F_T|$ was 0.040 for all multiple data with $|^{\lambda}F| > 3\sigma_F$. The $|^{\circ}F_A|$ values were then used to compute Patterson syntheses. After elimination of outlier and less significant data, maps could be interpreted as a two-site structure in space group *I222* (but not in the alternative $I2_12_12_1$). Harker sections for a map based on 30% of the 3-Å data are presented elsewhere (26). The local diad (4) relates the two sites to within 0.4 Å. Least-squares refinement of this model against 1187 $|^{\circ}F_A|$ values with $|^{\circ}F_A| > 3\sigma_F$ and $|^{\circ}F_A| < 100$ gave $R = 0.374$. A 5-Å Patterson map computed at the Photon Factory from a MAD fitting confirmed this model.

MAD Phasing Results. Our inability to interpret electron-density maps computed from MAD phasing of the SSRL data led us to a second attempt at the Photon Factory. Three-wavelength data were measured from 70- to 3.1-Å spacings. A total of 4618 reflection sets were collected. These data, after reduction and scaling, showed a pattern of average Bijvoet and dispersive differences that is consistent with theoretical expectation (Table 1). The symmetry R-value for centric $|^{\lambda}F|$ data having $|^{\lambda}F| > 3\sigma_F$ was 0.025. Analysis by MADLSQ led to a set of $|^{\circ}F_A|$ values and refinement against a restricted set of 354 reflections with $d > 3.3$ Å, $|^{\circ}F_A| > 5\sigma_F$, and $|^{\circ}F_A| < 300$ gave an R value of 0.281. This refined selenium structure specified $|^{\circ}F_A|$ and $^{\circ}\varphi_A$ for all reflections. These together with $|^{\circ}F_T|$ values from MADLSQ were then used to derive the *ABCD* coefficients for probability distributions from which figures-of-merit and centroid estimates of $^{\circ}\varphi_T$ were computed.

The distinction between the absolute configuration of selenium sites and its enantiomorph was clear-cut from the fidelity of molecular diad symmetry in the alternative electron-density maps. Correlation coefficients were computed for points within a sphere centered at the intersection of molecular diads. For a sphere of 22-Å radius and a map at 6-Å resolution, the distinction was 0.76 versus 0.18. By contrast, the alternative maps from the SSRL data gave correlation coefficients of 0.37 and 0.29 under these conditions. Due to low accuracy in the 3.3- to 3.1-Å shell, the Fourier synthesis for initial chain tracing was computed at 3.3-Å resolution. Molecular averaging refinement of the MAD phases was done in 10 steps from 6.0 Å to 3.1 Å with three cycles per step, and it led to increases in correlation coefficients from 0.81 to 0.89 at 6-Å resolution and from 0.62 to 0.75 at 3.1-Å resolution for points within a 16-Å-radius sphere.

Atomic Interpretation of Electron-Density Syntheses. Interpretable features were immediately apparent in the unaveraged, MAD-phased map at 3.3-Å resolution. Density associated with the selenium sites corresponded well with the known absolute structure of biotin (11), extended strands of density resembled polypeptide chain, rather featureless expanses depicted solvent regions and defined molecular boundaries, and of course the diad symmetry was evident (Fig. 2*A*). The averaged, phase-refined map enhances all of these aspects of the structure (Fig. 2*B*). Nevertheless, we concentrated on interpreting the map based purely on MAD information as a stringent test of the method. Working with a minimap stack of contoured transparent sheets, two of us independently traced the polypeptide chains of the two subunits in the asymmetric unit as a series of α-carbon (C^{α}) positions. One tracing was made without reference to the amino acid sequence and the other took it into account. These

Table 1. Anomalous diffraction difference ratios for Photon Factory data

	Observed ratio (d = 70–3.9 Å)			Observed ratio (d = 3.9–3.1 Å)			Expected ratio (d = ∞)		
	0.9000	0.9795	0.9809	0.9000	0.9795	0.9809	0.9000	0.9795	0.9809
0.9000	0.046 (0.037)	0.036	0.041	0.076 (0.048)	0.059	0.060	0.023 (0.000)	0.016	0.023
0.9795		0.046 (0.033)	0.026		0.067 (0.048)	0.052		0.025 (0.000)	0.007
0.9809			0.035 (0.027)			0.060 (0.045)			0.014 (0.000)

Observed and expected ratios at wavelengths of 0.9000, 0.9795, and 0.9809 Å were obtained. Bijvoet difference ratios (33) are given in diagonal elements with centric values in parentheses. Dispersive difference ratios (33) are given as the off-diagonal elements. Observed Bijvoet and dispersive difference ratios were computed as $\text{rms}(\Delta F_{\pm h})/\text{rms}(|F|)$ and $\text{rms}(\Delta F_{\Delta\lambda})/\text{rms}(|F|)$, respectively. Expected values were computed as $q(2f''(\lambda))$ for diagonal elements and $q|f'(\lambda_i) - f'(\lambda_j)|$ for off-diagonal elements where $q = (\sqrt{2N_T}Z_{\text{eff}})^{-1}$. $Z_{\text{eff}} = 6.7$ e (electrons) is the effective normal atomic scattering (33) at zero scattering angle and $N_T = 925$ is the approximate number of nonhydrogen atoms in core streptavidin.

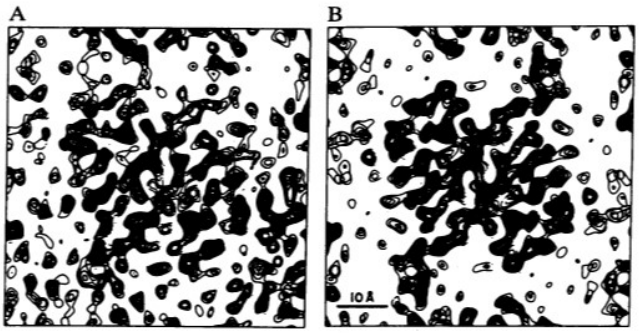

FIG. 2. Sections of electron-density distributions for selenobiotinyl streptavidin. (*A*) Map based exclusively on MAD phasing information ($m = 0.78$). (*B*) Map produced after molecular averaging refinement of the initial MAD phases ($m = 0.90$). Both maps are at 3.3 Å with contouring in intervals of 0.5σ starting at 1σ above the mean density level. Sections are perpendicular to the Q axis and include selenobiotins (densest features) and β-strands from two diad-related subunits. Five sections, taken at 1-Å intervals from 6 Å to 10 Å above the intersection of diads, are superimposed.

agreed closely, as shown elsewhere (26), except for one misinterpretation. The C^α backbone for the tracing that took cognizance of the sequence is shown in Fig. 3. These coordinates were used as the starting point for fitting a complete model using the averaged 3.1-Å map. The model from the fitted subunit was then transformed by diad symmetry to generate the other crystallographically distinct subunit.

The fitted atomic model was then subjected to restrained refinement (31) against all $|^{\circ}F_T|$ data in the range of spacings from 5 Å to 3.1 Å. Eleven cycles with an overall temperature factor reduced the R value from 0.488 to 0.316 for a model with stereochemistry typified by an rms deviation from bond ideality of 0.032 Å. Seven additional cycles with tightly restrained individual temperature factors (rms bonded B differences of 0.45 Å^2) and noncrystallographic symmetry (rms superposition of 0.15 Å), further reduced the R value to 0.293 and improved the bond ideality to 0.028 Å. This model subsequently served as the starting point for further refinement against a CuKα data set measured to higher scattering angles. The C^α backbone from the partially refined model is shown in Fig. 4 for the whole tetramer together with the selenobiotin ligands.

FIG. 3. Stereodrawing of the C^α backbone of the core streptavidin protomer. The C^α backbone from the initial tracing is shown in thin lines in comparison with the backbone from the latest refined model ($R = 0.177$ at 2-Å resolution) drawn in thick lines. The rms difference between these coordinates sets is 1.77 Å. The initial and final models have rms differences of 1.22 Å and 1.53 Å, respectively, from the model of Fig. 4. The view is down the molecular P axis (crystallographic **a** axis) with the R axis vertical. The amino-terminal strand is toward the reader and to the right of the longer carboxyl-terminal strand.

Molecular Description. The protomer of streptavidin is an elegantly simple β-barrel structure. Its polypeptide chain runs up and down in eight adjacent staves of a barrel such that the first and last β-strands are again adjacent and hydrogen-bonded to one another. The barrel is twisted as usual with each strand taking a right-handed helical course. The overall topology in streptavidin is like that in the retinol-binding protein family (34) and, by extension, in the 10-stranded fatty-acid-binding protein family as in P2 (35). However, the actual barrel structures themselves superimpose poorly.

The streptavidin tetramer has dihedral D_2 molecular symmetry (4) and in these crystals one diad coincides with the **a** axis. The other two molecular diads are displaced by 22° from **b** and **c** axes. We designate the molecular axes as P, Q, and R for those most nearly aligned with axes **a**, **b**, and **c**, respectively. The molecule extends about 54 × 58 × 48 Å along these respective molecular axes. Its surface, however, is not well described by an ellipsoid. Rather, it has an hour-glass figure with a waist perpendicular to the long Q axis. The barrel axes are roughly perpendicular to Q and are at approximately 35° from R. Strands 1–3 of the barrel are entirely superficial in the tetramer, but major parts of strands 4–7 are involved in the Q-axis interface and the P–R interface is completely mediated by strand 8 interactions. The interface between protomers related by the Q diad are very extensive and involve numerous side chains from the barrel strands. Interactions at the waist of the tetramer, about axes P and R, involve an intricate crossing of the four copies of strand 8 at the junctures of the two diads.

Biotin is buried quite deeply inside the barrel with only the carboxylate oxygens and the ureido-ring nitrogen involved in carboxyl-transfer reactions protruding to the outside. The carboxylates emerge from pockets on the molecular surface, in pairs separated by ≈20 Å on opposite faces surrounding the R axis. This suggests limits to the nature of conjugating groups for biotin labels used in streptavidin assays. Numerous hydrogen-bonding and van der Waals interactions are involved in the biotin binding. These include three hydrogen bonds to the carbonyl group buried deep within the barrel. There are also hydrogen bonds to the ureido nitrogens and carboxyl oxygens. Four tryptophans are in contact with each

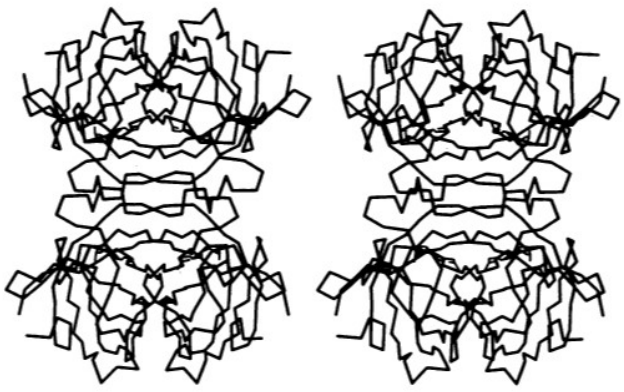

FIG. 4. Stereodrawing of the C^α backbone of the core streptavidin tetramer. This view is down the R axis with the Q axis vertical. Coordinates are from the model after refinement against the 3.1-Å $|^{\circ}F_T|$ data ($R = 0.293$). C^α backbones are drawn in thick lines and the selenobiotin molecules are shown in thin lines. Amino termini can be identified as being associated with strands 1–3, which are not involved in subunit interfaces.

Table 2. Comparisons between different phase sets

	Average phase discrepancy			
	MODEL	MAD	*ABCD*	AVG
MAD	56.9	0.0		
ABCD	57.2	8.3	0.0	
AVG	54.4	23.7	23.3	0.0
SSRL	82.2	72.8	73.2	72.3

Comparisons are based on all 4598 nonzero data to Bragg spacings of 3.1 Å. Phase sets designated as MAD, *ABCD*, and AVG derive from the Photon Factory data and are, respectively, from the algebraic analysis, from the probability formulation, and after molecular averaging refinement from the *ABCD* starting point. The SSRL phase set is that from the *ABCD* probability analysis. The MODEL phase set was calculated from the latest atomic model for all data from ∞ to 3.1 Å.

biotin molecule. Nearly all of the interactions are from the residues of a given subunit, and residues from seven β-strands and two loops contribute directly to this binding. However, one of the tryptophans is supplied by a subunit related by the *R* diad axis. This explains the reduced biotin affinity found with isolated subunits. Although each biotin site comprises interactions with just two chains, tetramer integrity appears to be essential since the *P–R* interface is a concerted association of all four subunits.

The initial C^{α} trace included positions 14–136 from the possible 13–139 sequence of the core streptavidin chain (4). Density for the terminal residues was weak, and thus the initial fitting for the full model was restricted to residues 14–133. Only residues 16–133 are included in our most recent model. These suffice to complete the β-barrel and leave the cleaved termini near one another at the end of the barrel opposite the biotin site and at corners of the tetramer (Fig. 4). There is ample space for the terminal peptides in the holo molecule, but we have no information about their disposition if indeed they are ordered.

MAD Phasing Evaluation. We restrict this report to descriptions of the MAD phase determination and the initial models from maps based on this phasing. However, starting from the model developed in this study, we have in fact refined selenobiotinyl streptavidin to $R = 0.177$ at 2-Å resolution with rms bond ideality of 0.014 Å. These results, as well as refinements of unligated molecules, confirm the general features of the initial model as is seen in the superposition of C^{α} backbones (Fig. 3). Moreover, phases calculated from this model serve as a useful benchmark (Table 2). Consistent with density map quality, phases from the Photon Factory data are substantially better than those from the SSRL data set. Possible sources of error in the latter include broad profiles due to crystal cracks and variations in illuminated crystal volume due to the large crystal size. The Photon Factory phasing was clearly excellent. The map at 3.3-Å resolution, based exclusively on MAD phasing, was easily as good as many MIR maps from our experience. These and other results (23) suggest that MAD phasing can be an advantageous alternative to the conventional MIR method in appropriate situations. The streptavidin success with one selenium per 126 residues also supports the suggestion that biologically produced selenomethionyl proteins could make the MAD method broadly applicable (36).

Structure factor data from the Photon Factory experiment and C^{α} coordinates from the model displayed in Fig. 4 are being deposited in the Protein Data Bank. An independent crystallographic analysis of streptavidin has produced similar results (37).

We thank John Horton for helping in data collection at Stanford, Celltech Ltd. for supplying streptavidin, Andrée Marquet and Jack Blount for providing selenobiotin, and Wilma Saffran for recovering the broken selenobiotin shipment. This work was supported in part by the National Institutes of Health. Synchrotron facilities used at SSRL are supported by the Department of Energy and by the National Institutes of Health. Synchrotron facilities used at the Photon Factory are supported by the Japanese Ministry of Education, Science and Culture.

1. Chaiet, L. & Wolf, F. J. (1964) *Arch. Biochem. Biophys.* **106,** 1–5.
2. Green, N. M. (1975) *Adv. Protein Chem.* **29,** 85–133.
3. Argarańa, C. E., Kuntz, I. D., Birken, S., Axel, R. & Cantor, C. R. (1986) *Nucleic Acids Res.* **14,** 871–882.
4. Pähler, A., Hendrickson, W. A., Gawinowicz Kolks, M. A., Argarańa, C. E. & Cantor, C. R. (1987) *J. Biol. Chem.* **262,** 13933–13937.
5. Gope, M. L., Keinänen, R. A., Kristo, P. A., Conneely, O. M., Beattie, W. G., Zarucki-Schulz, T., O'Malley, B. W. & Kulomaa, M. W. (1987) *Nucleic Acids Res.* **15,** 3595–3606.
6. Buckland, R. M. (1986) *Nature (London)* **320,** 557–558.
7. Bayer, E. A. & Wilchek, M. (1980) *Methods Biochem. Anal.* **26,** 1–45.
8. Fucillo, D. A. (1985) *Biotechniques* **3,** 494–501.
9. Weber, P. C., Cox, M. J., Salemme, F. R. & Ohlendorf, D. H. (1987) *J. Biol. Chem.* **262,** 12728–12729.
10. Bory, S. & Marquet, A. (1976) *Tetrahedron Lett.* **24,** 2033–2036.
11. DeTitta, G. F., Parthasarathy, R., Blessing, R. H. & Stallings, W. (1980) *Proc. Natl. Acad. Sci. USA* **77,** 333–337.
12. Hofmann, K., Titus, G., Montibeller, J. A. & Finn, F. M. (1982) *Biochemistry* **21,** 978–984.
13. Hendrickson, W. A. (1985) *Trans. Am. Crystallogr. Assoc.* **21,** 11–21.
14. Hendrickson, W. A. & Teeter, M. M. (1981) *Nature (London)* **290,** 107–113.
15. Sheriff, S. & Hendrickson, W. A. (1987) *Acta Crystallogr. B* **43,** 209–212.
16. Hendrickson, W. A. (1984) *Acta Crystallogr. A* **40,** C–3.
17. Hendrickson, W. A., Smith, J. L., Phizackerley, R. P. & Merritt, E. A. (1988) *Proteins* **4,** 77–88.
18. Karle, J. (1980) *Int. J. Quant. Chem.* **7,** 357–367.
19. Okaya, Y. & Pepinsky, R. (1956) *Phys. Rev.* **103,** 1645–1647.
20. Kahn, R., Fourme, R., Bosshard, R., Chaimdi, M., Risler, J. L., Dideberg, O. & Wery, J. P. (1985) *FEBS Lett.* **179,** 133–137.
21. Harada, S., Yasui, M., Murakawa, K., Kasai, N. & Satow, Y. (1986) *J. Appl. Crystallogr.* **19,** 448–452.
22. Korzun, Z. R. (1987) *J. Mol. Biol.* **196,** 413–419.
23. Guss, J. M., Merritt, E. A., Phizackerley, R. P., Hedman, B., Murata, M., Hodgson, K. O. & Freeman, H. C. (1988) *Science* **241,** 806–811.
24. Murthy, H. M. K., Hendrickson, W. A., Orme-Johnson, W. H., Merritt, E. A. & Phizackerley, R. P. (1988) *J. Biol. Chem.* **263,** 18430–18436.
25. Smith, J. L., Pähler, A., Murthy, H. M. K. & Hendrickson, W. A. (1987) *Acta Crystallogr. A* **43,** C-10.
26. Hendrickson, W. A., Horton, J. R., Murthy, H. M. K., Pähler, A. & Smith, J. L. (1988) in *Synchrotron Radiation in Biology*, ed. Sweet, R. M. (Plenum, New York), in press.
27. Phizackerley, R. P., Cork, C. W. & Merritt, E. A. (1986) *Nucl. Instrum. Methods A* **246,** 579–595.
28. Satow, Y. (1984) in *Methods and Applications in Crystallographic Computing*, eds. Hall, S. R. & Ashida, T. (Oxford Univ. Press, Oxford), pp. 56–64.
29. Hendrickson, W. A. & Lattman, E. E. (1970) *Acta Crystallogr. B* **26,** 136–143.
30. Jones, T. A. (1978) *J. Appl. Crystallogr.* **11,** 268–272.
31. Hendrickson, W. A. & Konnert, J. H. (1980) in *Computing in Crystallography*, eds. Diamond, D., Ramaseshan, S. & Venkatesan, K. (Indian Acad. Sci., Bangalore, India), pp. 13.01–13.25.
32. Templeton, L. K. & Templeton, D. H. (1988) *Acta Crystallogr. A* **44,** 1045–1051.
33. Hendrickson, W. A., Smith, J. L. & Sheriff, S. (1985) *Methods Enzymol.* **115,** 41–55.
34. Newcomer, M. E., Jones, T. A., Åqvist, V., Sundelin, J. & Unge, T. (1987) *EMBO J.* **3,** 1451–1454.
35. Jones, T. A., Bergfors, T., Sedzik, J. & Unge, T. (1988) *EMBO J.* **7,** 1597–1604.
36. Hendrickson, W. A. (1987) in *Crystallography in Molecular Biology*, ed. Moras, D. (Plenum, New York), pp. 81–87.
37. Weber, P. C., Cox, M. J., Salemme, F. R. & Ohlendorf, D. H. (1988) *American Crystallography Association Abstracts* (Am. Crystallogr. Assoc., Philadelphia), Ser. 2, Vol. 16, p. 103.